An animal-free bioprocess to synthesize 3D human matrix scaffolds using mesenchymal stromal cells

Shaianne N. Stein[1,2], Lorena R. Braid [1,2*]

[1]Simon Fraser University, Department of Molecular Biology and Biochemistry, Burnaby, BC, Canada

[2]Simon Fraser University, Centre for Cell Biology, Development and Disease, Burnaby, BC, Canada

*** Correspondence:**
Lorena R. Braid
lrbraid@sfu.ca

Keywords: Mesenchymal stromal cells (MSC), spheroid, decellularized matrix, extracellular matrix, collagen, basement membrane, animal component-free

Abstract

Basement membrane, the specialized extracellular matrix (ECM) that compartmentalizes endothelial and epithelial cells, is the final frontier in bioengineering. The fibrillar collagens (Col I and Col III) of the interstitial matrix are commonly used for tissue modeling, but the networking collagens that scaffold the basement membrane (human Col IV and Col VI) remain elusive. Commercial hydrogels like Matrigel that simulate basement membrane are ill-defined, dilute, variable and contain murine proteins. Here, we investigated whether human mesenchymal stromal cells (MSCs) could be used to produce 3D basement membrane scaffolds amenable to decellularization and downstream applications in bioengineering. Using a xeno-free, process, MSCs from placenta, umbilical cord, bone marrow and adipose tissues were cultivated as adherent multilayers or free-floating spheroids. Matrix assembly was assessed daily by fluorescence imaging and western blot, revealing *de novo,* systematic, matrix development. Notably, these scaffolds were rich in basement membrane-specific components Col IV and Col VI. Interestingly, we observed that MSCs produce distinct

25 combinations of Col IV alpha chains and other matrix components depending on their tissue of
26 origin. Ongoing work aims to combine this intrinsic Col IV patterning with other strategic process
27 parameters to refine basement membrane composition to resemble target tissues, and to develop
28 assays for processes like angiogenesis that incorporate relevant matrix biology as a variable and
29 readout.
30

Introduction

Bioengineering is a field of exponential biological innovation that is revolutionizing research and applied medicine. However, advancement of animal-free and human biomimetic biomaterials has been limited by the lack of raw materials to simulate the range of extracellular matrix (ECM) scaffolds that underlie human tissues. (Aisenbrey & Murphy, 2020; Perugini & Santin, 2021) In recent years, the critical role of ECM in fabricating high fidelity human organoids and tissues has become appreciated. (Jain et al., 2022; Kozlowski et al., 2021; Motta et al., 2023) The ECM not only serves as a scaffold that maintains the three-dimensional architecture of tissues but also influences cellular functions such as proliferation, differentiation, and migration through its biochemical composition and physical characteristics.(Olesen et al., 2021) Moreover, the mechanical properties of the ECM, such as stiffness and elasticity, significantly impact cellular behavior. (Black et al., 2008; Gonzalez-Fernandez et al., 2022; Saraswathibhatla et al., 2023; Thai et al., 2024)

Mammalian tissues and organs are scaffolded by two classes of ECM: (1) interstitial matrix and (2) basement membrane. (Pompili et al., 2021) Interstitial matrix is comprised mainly of the fibrillar collagens (I and III) and scaffolds the lamina propria, submucosa, muscular and serosa layers. (Pompili et al., 2021) The basement membrane is a specialized form of ECM located beneath the epithelial and endothelial cells that is scaffolded predominantly by the network forming collagen (Col), Col IV. (Khalilgharibi & Mao, 2021; Pompili et al., 2021) Basement membrane surrogates like Matrigel® and Cultrex™ are widely used in 3D culture. (Aisenbrey & Murphy, 2020; Kane et al., 2018) However, the biophysical, biochemical and functional properties of these matrix surrogates only distantly resemble human ECM. (Huang et al., 2021; Hughes et al., 2010; Kleinman & Martin, 2005; Kozlowski et al., 2021) These hydrogels are derived from murine Engelbreth-Holm-Swarm sarcoma (Jain et al., 2022; Kozlowski et al., 2021; Motta et al., 2023) and can contain up to 1800

55 different mouse proteins (Hughes et al., 2010) which introduce xenogeneic contaminants that that
56 interfere with experimental veracity and that are incompatible with transplant into humans.
57 (Aisenbrey & Murphy, 2020; de la Vega et al., 2019) While these and other biomaterials like bioinks
58 contain soluble matrix components, they lack the structural organization that provides essential cues
59 for tissue development and organization. (Tuftee et al., 2024) Thus, there is a critical need for
60 animal-component free matrix scaffolds that recapitulate the architecture of native tissues.
61
62 Several approaches have been explored to address this limitation. Tissues and organs from animals
63 and from human cadavers can be decellularized to yield intact matrix scaffolds for selective
64 reseeding to create tissue models for experimentation (Duisit et al., 2018; Jin et al., 2022; Johnson et
65 al., 2016) and transplant. (Griffith et al., 2022; Shaheen et al., 2020) Similarly, homogeneous and
66 multicellular spheroids (microtissues) can be cultivated to facilitate 3D ECM synthesis followed by
67 decellularization for downstream applications. (Chen et al., 2025; Chiang et al., 2021; Fonseca et al.,
68 2023; Malakpour-Permlid et al., 2021; Y. Zhang et al., 2023) A recent study showed that human lung
69 and cardiac fibroblasts from healthy and diseased donors could be used to synthesize matrix scaffolds
70 that recapitulate the architectural features of normal and diseased lungs and hearts, respectively.
71 (Fonseca et al., 2023; Franco-Barraza et al., 2016) Other matrix-producing cell types, including
72 mesenchymal stromal cells (MSCs), epithelial, hepatocytes and endothelial cells have also proven
73 useful for producing 3D matrix scaffolds with various compositions and architecture. (Fonseca et al.,
74 2023; Pompili et al., 2021; Smith et al., 2020; Tao et al., 2020) Together, these data suggest that the
75 range of tissue-specific matrices found throughout the human body could potentially be synthesized
76 *in vitro* by strategic selection of cell type for 3D culture. Further refinement may also be achieved by
77 tuning environmental conditions by addition of small molecules (Tong et al., 2018), growth factors
78 (Gonzalez-Fernandez et al., 2016; Malakpour-Permlid et al., 2021; Seif-Naraghi et al., 2012) and

macromolecular crowding, for example. (Assunção et al., 2020; Chiang et al., 2021; Tao et al., 2020) Several groups have characterized how different decellularization techniques affect matrix structure and function, enabling researchers to select detergents that allow them to preserve the relevant matrix attributes necessary for their applications. (Kim et al., 2022; Crapo et al., 2011; Fonseca et al., 2023; Gilpin & Yang, 2017; Marinkovic et al., 2016, 2020; Park et al., 2018; Prewitz et al., 2013; Rakian et al., 2015).

Despite the rich potential to exploit human cells to synthesize ECM *in vitro*, most studies to date include xenogeneic components like fetal bovine serum (FBS) for cell culture. FBS remains the most widely used cell culture supplement due to its low cost and rich source of nutrients, growth factors and hormones to support mammalian cell growth and proliferation. (M. Baker, 2016b; Hemeda et al., 2014; Jung et al., 2010; Liu et al., 2023) However, many growth factors are sequestered in the matrix for on-demand release by proteases during tissue remodeling, injury and inflammation. (Keppie et al., 2021; Zhang et al., 2017) Thus, ECM cultivated in the presence of FBS contains embedded proteins of bovine origin, a concern exacerbated by the reported batch-to-batch variability of FBS. (M. Baker, 2016b, 2016a; Hemeda et al., 2014; Jung et al., 2010; Liu et al., 2023) Human platelet lysate (hPL) is a non-xenogeneic alternative to FBS for human cell culture but is also plagued by donor variability (Hemeda et al., 2014; Jung et al., 2010; Becherucci et al., 2018; Palombella et al., 2022) and is therefore not ideal for experiments and processes that require stringent reproducibility. Chemically defined culture media are emerging as an important alternative to ensure reproducible bioprocess conditions. However, these formulations are not as nutrient-rich as FBS or hPL-containing products, resulting in overall blunted cell performance. (Hemeda et al., 2014; Jung et al., 2010; Xu et al., 2020; Spoerer et al., 2025).

103 Here we tested whether human MSCs could synthesize *de novo* 3D ECM scaffolds in an animal
104 component-free workflow. We adopted a quality-by-design approach to select only defined and
105 qualified reagents, including MSCs, that are available in GMP-compliant formulations for further
106 manufacturing. Several studies have already shown that MSCs synthesize a wide array of ECM
107 constituents (Chen et al., 2025; Maia et al., 2014; Novoseletskaya et al., 2020; Sagaradze et al., 2020;
108 Yin et al., 2024), and we previously reported that many of the potential biomarkers that distinguish
109 MSCs from fibroblasts are linked to the matrisome. (Wiese & Braid, 2020) Fibroblasts are
110 components of interstitial tissue and are programmed to synthesize interstitial matrix containing the
111 fibrillar collagens 1 and 3 amongst others. (Kumada & Zhang, 2010; Wilks et al., 2018) Here we
112 show that perinatal (umbilical cord (UC) and placental (PL)) and adult (adipose (AD) and bone
113 marrow (BM)) derived MSCs synthesize 3D ECM in suspended and adherent chemically-defined
114 cultures. The composition of the matrices varies by MSC tissue of origin and can include basement
115 membrane-like scaffolds enriched for the networking collagen Col IV.
116

117 **Materials and Methods**

118 2.1 Cell source

119 High quality human MSCs were obtained from commercial sources. UC were provided by Tissue
120 Regeneration Therapeutics (TRT), Inc. (Toronto, Canada). UC MSCs were isolated from the
121 perivascular Wharton's jelly of healthy term (>37 weeks) umbilical cords from 1 male and 1 female
122 infant delivered by C-section and cryopreserved at mean population doubling level (mPDL) 4.87. AD
123 and BM MSCs from female donors were obtained from RoosterBio Inc. (Frederick, MD) at 8.9 and
124 8.8 mPDL respectively. PL MSCs from a female donor was obtained from OrganaBio (Miami, FL)
125 at PDL 8.39. Experiments were performed using one donor population per tissue of origin.

126

127 2.2 Cell culture and maintenance

128 For cell expansion, MSCs were seeded at a density of 1,333 cells (UC MSCs) and 3,000 cells (AD,
129 BM, PL MSCs)/cm^2 in chemically defined phenol red-free MSC NutriStem XF® complete growth
130 media (Sartorius AG, USA). Culture-ware was pretreated with 2.67µg/cm^2 Col IV from human
131 placenta (MilliporeSigma) to facilitate adherence. Cells were maintained in physioxia at 37°C, 5%
132 CO_2, 5% O_2 and 80% relative humidity. At 70-80% confluence, MSCs were washed briefly with
133 Dulbecco's phosphate buffered saline (DPBS; MilliporeSigma) and enzymatically detached by brief
134 incubation with TrypLE Select (ThermoFisher Scientific, Waltham, MA). Upon complete
135 dissociation, an equal volume of media was added to the cell suspension and cells enumerated using
136 the CellDrop Fluorescent Cell Counter (DeNovix Inc., USA). Cells were pelleted by centrifugation at
137 150 x *g* for 5 minutes and the cell pellet resuspended in fresh chemically defined media before re-
138 seeding. All experiments were performed using MSCs between PDLs 16-24.

139 2.3 Generation of 3D MSC adherent multilayers

140 MSCs were expanded and maintained to harvest an appropriate number of cells for experiments.
141 High-density MSCs (7,813 cells/cm^2) were seeded into 24 well plates in chemically defined media
142 with media changes every 2-3 days and maintained at 37°C, 5% CO_2, 5% O_2 and 80% relative
143 humidity. At specified timepoints (days 1, 2, 4 or 7 after seeding), MSCs were washed with DPBS
144 and then decellularized (see section 2.5) for subsequent immunostaining.

145

146

147

148 2.4 Self-assembled spheroids

149 Spheroids were generated using a protocol adapted from Li et al (Li et al., 2021): 96-well plates were
150 coated with 75µl of sterile 1% agarose (w/v) and allowed to solidify at room temperature. Coated
151 plates were used immediately or stored up to 1 week in 80µl DPBS per well. DPBS was aspirated
152 prior to seeding. MSCs were suspended in culture media at a concentration of 437,500 cells/ml
153 (35,000 cells/well). 80µl of cell suspension was added to the coated wells and spheroids were
154 allowed to spontaneously aggregate over 4 days. To generate spheroids of different sizes, UC MSCs
155 were cultivated using initial cell counts of 7,000, 15,000, 35,000 or 75,000 MSCs per well.
156
157 To quantify differences in spheroid morphology across MSC tissue sources, AD, BM, PL and UC
158 MSCs spheroids were nucleated using 35,000 cells/well. Phase contrast images were captured on
159 days 1, 2 and 4 using an Echo Revolve inverted microscope (ECHO Inc., USA) with 10X objective
160 for morphometric analysis.
161

162 2.5 Decellularization

163 Adherent multilayered MSCs were decellularized on days 1, 2, 4 and 7 after seeding. Briefly, 24 well
164 plates were rinsed twice in DPBS, then incubated in decellularization solution (20mM NH_4OH +
165 0.5% Triton-X100 plus 1X cOmplete^{TM} EDTA-free protease inhibitor cocktail (Roche) for 5 minutes
166 at 37°C, 5% CO_2, 5% O_2 and 80% relative humidity.
167
168 Spheroids were washed twice in DPBS for 5 minutes each then incubated in decellularization
169 solution for 30 minutes at 37°C, 5% CO_2, 5% O_2 and 80% relative humidity. To remove residual
170 DNA, the decellularized spheroids were washed twice more in DPBS, then treated with 50kU of

171 DNAseI plus EDTA-free protease inhibitor diluted in water for 30 minutes at 37°C, 5% CO_2, 5% O_2
172 and 80% relative humidity.

173 2.6 Immunofluorescence

174 Immunofluorescence imaging of adherent multilayer scaffolds was performed on cellularized and
175 decellularized samples. Wells were rinsed, fixed with 10% neutral buffered formalin for 10 minutes
176 and then permeabilized with PBT (1X DPBS + 0.1% Triton-X100) for 10 minutes followed by two
177 phosphate buffered saline (PBS) rinses. Wells were then blocked with 10% normal donkey serum
178 (MilliporeSigma) diluted in PBST (PBS + 0.1% Tween-20) for 30 minutes. Primary antibodies
179 against human collagen-IV (Col IV, 1:200, NovusBio NB120-6586), laminin (LM, 1:200, NovusBio
180 NB300-144,), fibronectin (FN, 1:200, NovusBio AF1918), and collagen-VI alpha 1 (Col VI, 1:200,
181 NovusBio NB120-6588) were diluted in antibody dilution buffer (PBS + 0.1% Triton-X100 with 1%
182 bovine serum albumin (BSA)) (MilliporeSigma) and incubated with the sample overnight at 4°C.
183 Cells were washed 3 times for 5 minutes each with PBS at room temperature, then incubated for 1
184 hour at room temperature with secondary antibodies (donkey anti-Rabbit IgG (H+L) conjugated to
185 AlexaFluor™ 647 (Invitrogen A32795) or donkey anti-Sheep IgG conjugated to AlexaFluor™ 594
186 (Invitrogen A110106)) diluted 1:1000 in antibody dilution buffer. Cells were rinsed twice with PBS
187 and then stained with 4',6-diamidino-2-phenylindole (DAPI, 1:4000, MilliporeSigma) for 2 minutes
188 at room temperature before washing 3 times for 5 minutes each in PBS.
189

190 Images were captured using a Nikon ECLIPSE Ti2-E inverted microscope with the 20X objective
191 lens with 32X averaging on NIS Elements software (Nikon Instruments, Inc., USA). Images were
192 edited using FIJI (v1.54k; (Schindelin et al., 2012)). Wells corresponding to days 1 and 2 were edited
193 to remove background and visualize weak signal. Raw images were imported into FIJI as 16-bit,

194 greyscale images and the brightness and contrast of each image optimized: FN minimum and
195 maximum levels were set to 185 and 400, respectively; Col IV minimum and maximum levels were
196 set to 170 and 600, respectively; Col VI minimum and maximum levels were set to 120 and 275,
197 respectively; LM minimum and maximum levels were set to 115 and 540, respectively. Images
198 taken on days 4 and 7 were comparably adjusted to maintain consistency between timepoints. FN
199 minimum and maximum levels were set to 160 and 250, respectively; Col IV minimum and
200 maximum levels were set to 145 and 275, respectively; Col VI minimum and maximum levels were
201 set to 125 and 200, respectively; LM minimum and maximum levels were set to 115 and 190,
202 respectively. Z-stacked images were taken using a Nikon A1R Laser Scanning Confocal microscope
203 equipped with a Plan Fluor 40X Oil DIC H N2 lens with cellularized UC MSCs after 7 days in
204 culture.
205
206 Decellularization efficiency was measured using FIJI. DAPI 16-bit images were imported and
207 threshold with black background was set for the cellularized (913-65535) and decellularized (1600 or
208 2724- 65535) respectively. A gaussian blur with sigma factor 2 was applied with auto thresholding
209 set to "default dark". The images were masked based on the thresholding values, and the "analyze
210 particles" tool was used to obtain nuclei count. Intact nuclei were counted from at least 10 fields of
211 view per each of 3 decellularized wells and per 1 cellularized well in each experiment.
212 Decellularization efficiency was calculated as the percent of nuclei in decellularized wells compared
213 to cellularized wells.

214 2.7 Morphometric analysis

215 Images were acquired on days 1, 2 and 4 as described in section 2.4 and processed using Adobe
216 Photoshop 2023 (24.0.1, Adobe, USA). Spheroids were selected using Object Selection. In cases

217 where the background was too high for auto-selection, the Magnetic Lasso tool was used to manually
218 trace the spheroid perimeter. The background replaced with grey as a separate layer on Photoshop to
219 restrict calculations of each spheroid. For the initial spheroid seeding density experiments, the Ruler
220 tool was used to measure spheroid diameter after 4 days in culture. Next, the Measure tool was used
221 to automatically quantify spheroid area, perimeter and circularity. At least 19 spheroids per
222 biological replicate, per tissue source were quantified.

223 2.8 Western blot

224 Total protein was collected from at least 15 pooled, decellularized and DNAseI-treated spheroids per
225 tissue source and replicate. Decellularized spheroids were washed twice with DPBS then submerged
226 in 75µl radioimmunoprecipitation assay (RIPA) buffer and immediately flash frozen in liquid
227 nitrogen and stored at -80°C until use. 3D matrices were solubilized by 3 rounds of sonication at 10%
228 amplitude for 30 seconds (1 second on, 1 off). Protein concentration was determined using
229 Bicinchoninic acid assay (BCA; MilliporeSigma). Samples were diluted and prepared in 6X Laemmli
230 buffer to load 3ug of total protein in 10µl per lane then boiled at 95°C before loading on an 8% gel.
231 Proteins were subjected to electrophoresis for 1.5 hours at 140V. Size fractionated proteins were
232 transferred to a nitrocellulose membrane overnight at 4°C. The membrane was incubated with
233 primary antibody solution (rabbit anti-human col IV (1:1000, NovusBio, NB120-6586), rabbit anti-
234 laminin (1:1000, NovusBio, NB300-144), rabbit anti-col VI alpha 1 (1:2000, NovusBio NB120-
235 6588), rabbit anti Col I (1:500, Abcam ab34710), sheep anti-fibronectin (1:3000, NovusBio AF1918)
236 or rabbit anti-elastin (1:3000, Invitrogen PA5-99418) overnight at 4°C. Membranes were then
237 washed twice in 1X TBST for 10 minutes each, followed by blocking for 10 minutes each in 5%
238 skim milk, and 5% BSA for elastin. Secondary antibodies (goat anti-rabbit IgG, H+L chain specific
239 peroxidase conjugate (1:3000, Millipore Sigma 401393), rabbit anti-sheep IgG (H+L) secondary

240 antibody (1:4000,Invitrogen 61-8620) or AMDEX™ goat anti- rabbit horseradish peroxidase
241 conjugate (1:3000, Cytiva RPN4301) were diluted in blocking solution and added to the membrane
242 for 1 hour at room temperature. Membranes were washed four times in 1X TBS + 0.1% Triton-X100
243 (TBST) and visualized using UltraScence Pico Ultra Western Substrate (FroggaBio). Western blots
244 were imaged using an Amersham™ AI600 Imager (GE HealthCare Technologies, USA).
245
246 2.9 Statistical analyses
247
248 Statistical analysis was carried out using Prism 10.3.1 (GraphPad Software, LLC). Significant
249 differences were calculated using student's t-test (decellularization efficiency), 2-way analysis of
250 variance (spheroid morphometrics) and Kruskal-Wallis test (spheroid initial seeding density). Error
251 bars represent standard deviation (SD) ± of the calculated means. ns = non-significant $P>0.05$, * $P \leq$
252 0.05, ** $P \leq 0.01$, *** $P \leq 0.001$ and **** $P \leq 0.0001$. All experiments were performed 3
253 independent times.
254
255 **Results**

256 *Multilayered UC MSCs produce 3D matrices in chemically defined media*

257 We first asked whether our previously documented expression of matrisome genes by UC MSCs
258 (Wiese & Braid, 2020) correlated with protein synthesis and could result in *de novo* production of
259 matrices containing the basement membrane collagen Col IV in chemically defined conditions. UC
260 MSCs were cultured in adherent multilayers followed by decellularization to assess ECM biogenesis.
261 Ammonium hydroxide decellularization cleared 95.3% of nuclei, proving highly effective (Fig.S1).
262 We then analyzed the deposition of select adhesive (fibronectin, laminin) and structural (Col IV) matrix

263 proteins over time by immunofluorescence. In the multilayer scaffolds, fibronectin was the most
264 prevalent matrix component at Day 1 and increased in abundance and architectural complexity through
265 day 7 (Fig. 1A, B). Laminin and Col IV were not detectable until Day 2, after which both proteins
266 accumulate in networked structures through day 7 (Fig. 1A, B). Z-stacked cross-section views of day
267 7 cellularized cultures (Fig. 1C) reveal a matrix depth of approximately 8µm, with fibronectin
268 interspersed throughout the scaffold (Fig. 1D). Lysl oxidase-like 2 (LOXL2), an ECM crosslinking
269 enzyme and important for Col IV stabilization was used as a cytoplasmic marker to delineate MSCs
270 (white) depicting them directly interacting with the fibronectin matrix (Fig. 1C, D).
271

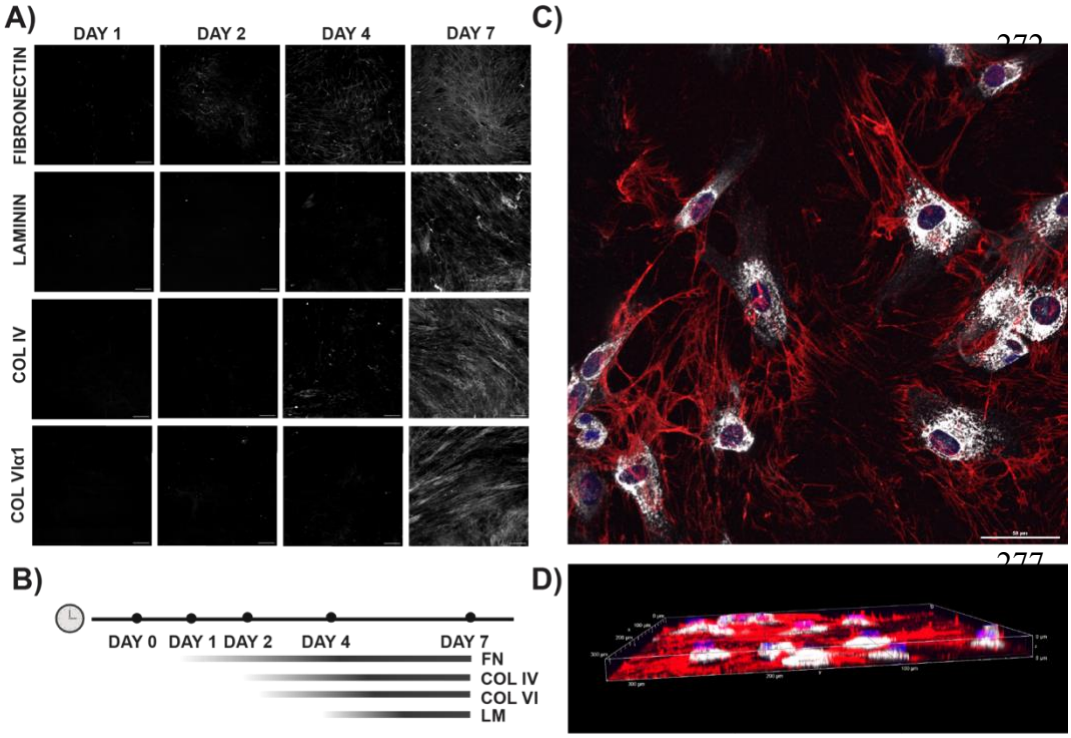

279 **Figure 1: High-density UC MSC cultures construct 3D matrices.** (A) Fibronectin is first detected
280 by immunogenic staining 2 days after seeding, followed by Col IV on Day 4. Laminin and Col VI are
281 not readily detected until Day 7, when all 4 analytes are visible components of an organized matrix
282 structure. Scale bar = 100µm (B) Schematic summarizing the temporal synthesis of ECM
283 components depicted in (A). (C) Z-stacked maximum intensity projection of cellularized adherent

284 multilayers reveal networks of fibronectin (red) networks intercalating between MSCs (white). (D)
285 3D adherent multilayer displayed in maximum intensity projection cross-section (volume) view
286 shows 8 µm matrix thickness in the Z-plane. Red: fibronectin, white: LOXL2 (cytoplasmic marker),
287 blue: DAPI (nuclear marker). Data shown is representative from a dataset of n=3 independent
288 experiments with 5-6 fields of view per experiment.

289 *MSCs from different human tissues self-assemble into 3D spheroids in chemically defined media*

290 Having confirmed that UC MSCs can produce Col IV-positive matrix with scaffolded architecture,
291 we next examined whether MSCs from adult (AD, BM) and perinatal (PL, UC) tissues could
292 construct *de novo* 3D matrix as spheroids when cultured in chemically defined media. Within four
293 days of high-density seeding on agarose-coated 96-well plates, MSCs from both adult and perinatal
294 tissues formed a single free-floating spheroid in each well (Fig. 2A). A small number of
295 unincorporated cells remained in solution and formed micro-aggregates or attached to the wall of the
296 well, particularly in AD MSC cultures (not shown).
297

298 The morphometric uniformity and reproducibility of the resulting spheroids were assessed within
299 tissue each source and between tissue sources. The spheroids become more uniform over time.
300 Circularity (where 1.0 is a perfect circle) increases from day 1 to day 4 by 11-15% for each MSC
301 type, resulting in average circularities of 0.84, 0.78, 0.80 and 0.80 by day 4 for AD, BM, PL and UC
302 MSCs, respectively (Fig. 2B, C). Circularity was accompanied by compaction, as the spheroids
303 significantly decreased in area (Fig. 2D, E) and perimeter (Fig. 2F, G). Interestingly, the rate and
304 extent of compaction varied between MSCs from different tissues (Fig. 2C, E, G) where PL MSCs
305 exhibited the least compaction (mean area $2.29E^5 \mu m^2$), followed by AD MSCs (mean area

306 $2.09E^5 \mu m^2$). UC MSCs and BM MSCs produced the most compact spheroids with mean area

307 $1.60E^5 \mu m^2$ and $1.20E^5 \mu m^2$, respectively.

308

309 We next investigated how initial cell density might influence spheroid self-assembly. Spheroids were

310 nucleated using 7,000, 15,000 35,000 and 75,000 MSCs per well. (Fig. 3A) Irrespective of seeding

311 density, all spheroids successfully self-aggregated. Spheroid size increased relative to seeding

312 density, but not linearly (Fig. 3B). All spheroids were visible by eye with diameters ranging from

313 326 to 707µm (Fig. 3A). With the exception of the largest aggregates nucleated with 75,000 cells,

314 spheroids could be aspirated using a P1000 pipette without shearing. On the other hand, the smallest

315 spheroids were challenging to visualize and manipulate. Considering these practical limitations, as

316 well as reported oxygen diffusion limits (Murphy et al., 2017), we selected spheroids nucleated using

317 35,000 MSCs and cultured to day 4 for the remainder of the study.

318

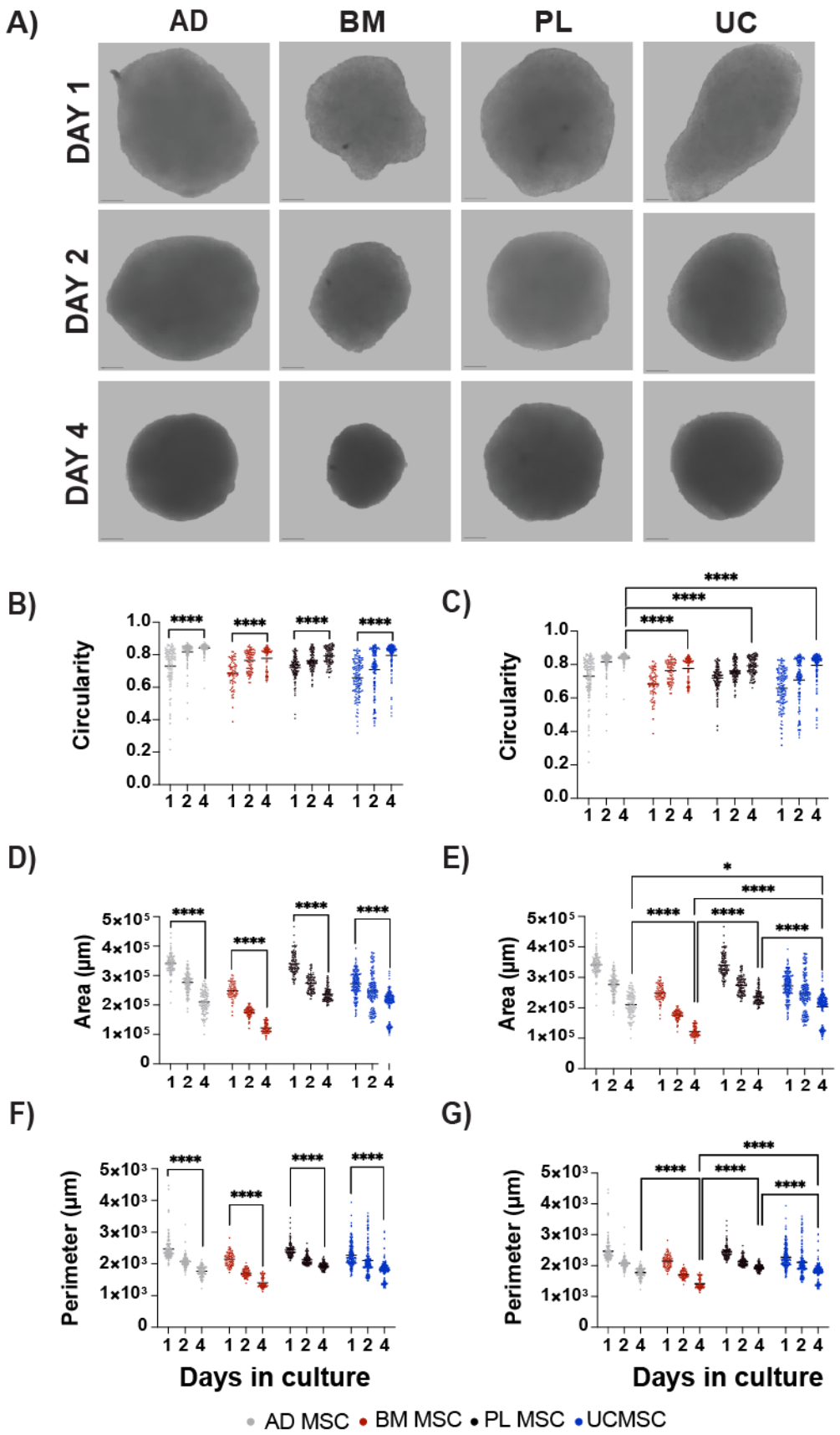
A)
AD
BM
PL
UC
DAY 1
DAY 2
DAY 4
B)
Circularity
C)
Circularity
D)
Area (µm)
E)
Area (µm)
F)
Perimeter (µm)
G)
Perimeter (µm)
Days in culture
Days in culture
AD MSC
BM MSC
PL MSC
UCMSC

321 **Figure 2: MSC tissue source influences spheroid morphology.** A) Spheroids from AD, BM, PL
322 and UC MSCs display variable morphology after 4 days in culture. MSC spheroids became more
323 uniform over time as shown by changes in circularity where 1.0 is a perfect circle (B) within tissue
324 sources and (C) across tissue sources. The increase in circularity is accompanied by an increase in
325 compaction and a significant decrease in area (D) within tissue sources and (E) across tissue sources
326 along with a significant decrease in perimeter (F) within tissue sources and (G) across tissue sources.
327 At least 19 spheroids per tissue source were analyzed per experiment. Each datapoint corresponds to
328 one spheroid from n=3 independent experiments. Scale bar = 100µm.
329

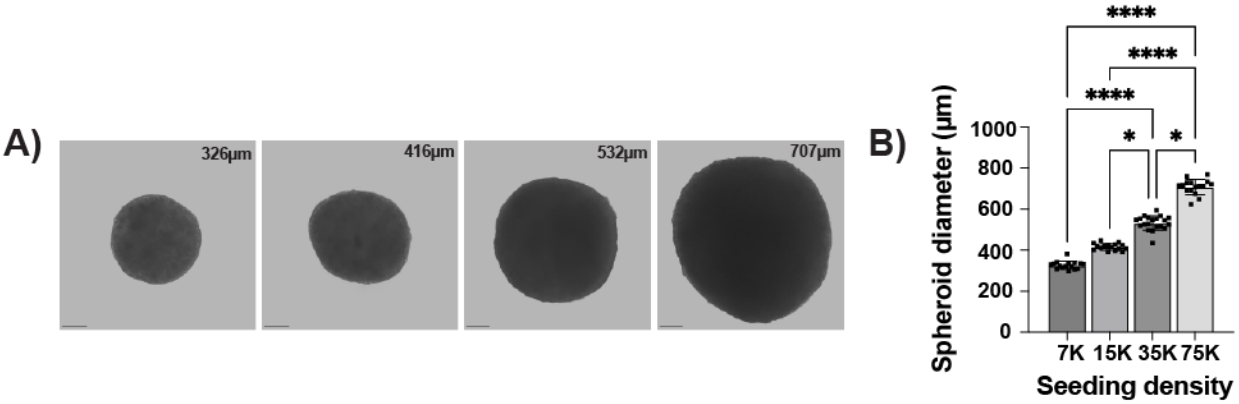

330
331 **Figure 3: Spheroid diameter increases with initial seeding density.** Spheroids were seeded using
332 7,000, 15,000, 35,000 or 75,000 US MSCs and cultivated for 4 days. (A) Diameter (upper right
333 corner) is the average measurement for each group. (A, B) Spheroid diameter (µm) increased with
334 seeding density.
335 Representative images are from n=3 independent experiments. Scale bar = 100µm.
336

337 *MSCs from different tissue sources produce different levels of matrix components*

338 We then examined how tissue of origin might influence the ability of MSCs to produce basement
339 membrane-like ECM. Decellularized 3D spheroids were solubilized, normalized to total protein and

340 analyzed by western blot. Only UC- and AD-derived matrices contained detectable levels of all the
341 analytes, although Col IV and elastin were less represented in the AD-derived scaffolds. All the
342 analytes except elastin were also detected in PL-derived ECM, although Col I was more prevalent
343 than in the other matrices. The matrix produced by BM MSCs was markedly different and comprised
344 mainly of fibronectin with little to no Col I, Col IV or elastin. Interestingly Three Col I isoforms,
345 sized 140, 120 and 115 kDa, were produced at different levels by AD, PL and UC MSCs. While AD
346 MSCs produced similar levels of the isoforms, PL MSCs preferentially synthesized the 120 and 115
347 kDa isoforms and the 115kDa isoform was the most prominent Col I isoform in UC MSC matrix.
348

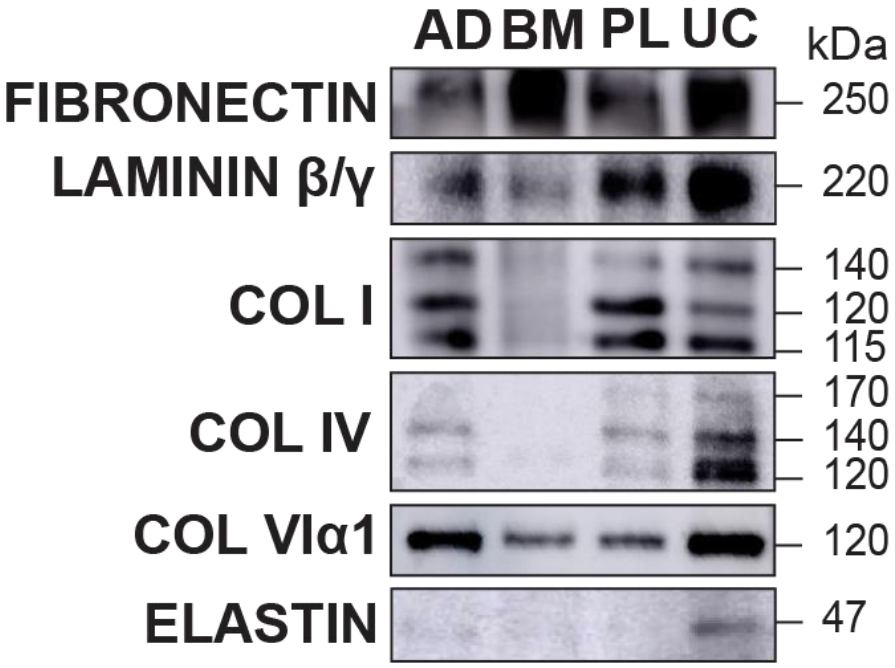

349
350
351 **Figure 4: MSC from different tissues produce compositionally distinct matrices.** Relative
352 abundance of basement membrane proteins in decellularized AD, BM, PL or UC MSC spheroids
353 were analyzed by western blot. Samples were normalized by total protein (3µg/lane). UC MSC
354 matrices were enriched for all the tested basement membrane factors, although AD and PL MSCs
355 synthesized relatively more Col I. AD and PL MSCs also produced many basement membrane
356 factors although Col IV levels were substantially less than the other analytes. By contrast, matrix

357 from BM MSCs was relatively enriched for fibronectin, with negligible levels of Col I and Col IV.
358 Representative data from n=3 independent experiments.
359
360 **Discussion**
361
362 There is a critical need for functional human matrix components to support the next generation of
363 high-fidelity tissue models for experimental use and transplant. (Catarino et al., 2022; Liu et al.,
364 2023; Naderi-Meshkin et al., 2023; Schneider et al., 2023) Moreover, there is a paucity of intact and
365 functional basement membrane biomaterials to recapitulate the complexity of human tissues, and
366 more importantly, to facilitate vascularization.(Chan et al., 2016; Marrella et al., 2018; Minor &
367 Coulombe, 2020; Zhao et al., 2022) Here we report that the intrinsic architectural capacity of MSCs
368 (Kim et al., 2023; Marinkovic et al., 2020; Novoseletskaya et al., 2020; Ushakov et al., 2024; Yang et
369 al., 2024), which occupy perivascular basement membrane niches *in vivo* (Caplan, 2017; Corselli et
370 al., 2013; Kang et al., 2010) can be leveraged to synthesize basement membrane-type matrices in a
371 chemically defined bioprocess.
372
373 We performed a temporal analysis of extracellular matrix deposition and spheroid formation, studies
374 that are reportedly under-represented in the literature. (Fuentes et al., 2022) We found that MSCs
375 build 3D matrix in an organized fashion, beginning with synthesis of fibronectin. The fibronectin
376 fibers are then overlaid with laminin and Col IV, accompanied by ongoing fibronectin incorporation,
377 which recapitulates the hierarchical pattern of basement membrane synthesis *in vivo*. (Pompili et al.,
378 2021) We also documented increased spheroid organization and compaction over time, although the
379 degree of compaction was different between MSC cultures from different tissue sources. Compaction
380 is a natural developmental process that indicates organotypic self-organization. (Baker & Chen,

381 2012; Domnina et al., 2020) Spontaneous compaction, as observed here, is mainly driven by ECM
382 structure and stiffness. (Efremov et al., 2021; Jahin et al., 2023; Kosheleva et al., 2023) we found that
383 BM MSC-derived spheroids were significantly more compact, contained relatively more fibronectin
384 and lacked the networking Col IV. These data suggest that BM MSC-matrices are considerably
385 stiffer than matrices derived from UC, PL and AD MSCs, may contain high levels of other fibrillar
386 collagens like Col III, and together are not suitable for synthesis of basement membrane-type
387 matrices.
388
389 Indeed, we found that the synthesis and relative abundance of basement membrane components was
390 influenced by MSC tissue of origin. Based on previous studies (Marinkovic et al., 2016, 2020;
391 Rakian et al., 2015), including our reports that UC MSCs express significantly higher levels of the
392 non-fibrillar basement membrane collagens (Col IV and Col VI) than fibroblasts (Wiese & Braid,
393 2020) and BM MSCs (Wiese et al., 2022), this outcome was anticipated. However, our results differ
394 from some previous reports. For example, the Chen group reported that decellularized BM MSC
395 scaffolds contained Col IV, while AD MSC scaffolds did not (Marinkovic et al., 2020), which is the
396 inverse of our results. These disparate outcomes may be the consequence of different media
397 formulations and FBS supplements (Bartosh et al., 2010; Cesarz & Tamama, 2016; Chen et al., 2025,
398 2025; Chiang et al., 2021; Fuentes et al., 2022; Lee et al., 2016; Yin et al., 2024). Only a few studies
399 have investigated ECM synthesis in serum-free conditions (Choi et al., 2021; Rakian et al., 2015),
400 while even fewer have used fully xeno-free processes. (Bauman et al., 2018)
401
402 Environmental conditions like oxygen tension also influence matrix synthesis. (Kumar et al., 2018;
403 Lee et al., 2016; Satyam et al., 2016) For example, a recent study showed that human articular
404 chondrocytes cultured at physiological oxygen tension (5% O_2) produced thicker matrices wither

405 increased deposition of glycosaminoglycans and Col II as well as increased tensile strength. (Dennis
406 et al., 2020) MSC spheroids cultured under hypoxia (2% O_2) produced more laminin, fibronectin and
407 Col I compared to spheroids cultured at ambient (~20%) O_2. (Shearier et al., 2016) Since MSCs were
408 cultivated under 5% O_2 in our study, oxygen tension may be a key differential that contributes to the
409 disparate outcomes between our data and other studies that maintain MSCs at ambient O_2 tension.
410

411 This study provides proof-of-concept that human MSCs can be leveraged to produce 3D matrices,
412 including scaffolds enriched for basement membrane components, in an animal-component free and
413 defined bioprocess. Subsequent work will use proteomics to comprehensively characterize the
414 structural and signaling composition of the scaffolds. Biophysical analyses will provide further
415 insight into how the biomechanics of these MSC-derived matrices and will inform tuning of culture
416 conditions to more closely recapitulate *bona fide* ECM. The results herein are an in important step
417 forward in the pursuit of high fidelity, functional tissue models for disease modeling, drug discovery
418 and regenerative medicine.

419 **Conflict of Interest**

420 *LRB is founder and CSO of Aurora BioSolutions Inc. SNS has no conflicts to declare. The authors*
421 *declare that the research was conducted in the absence of any commercial or financial relationships*
422 *that could be construed as a potential conflict of interest*.

423 **Author Contributions**

424 SNS: Collection and/or assembly of data, data analysis and interpretation, manuscript writing, critical
425 review of the manuscript and final approval of manuscript. LRB: Conception/design, assembly of

426 data, data analysis and interpretation, manuscript writing, critical review of the manuscript and final
427 approval of manuscript.

428 **Funding**

429 This project was funded by an NSERC Discovery Grant to LRB. Additional operating funds were
430 provided by a Canada Research Chair (Tier 2) in MSC Biology awarded to LRB.

431 **Acknowledgments**

432 We thank Tissue Regeneration Therapeutics Inc. (TRT), Toronto, Canada, for provision of human
433 umbilical cord perivascular cells.

434 **Supplemental Figure**

435

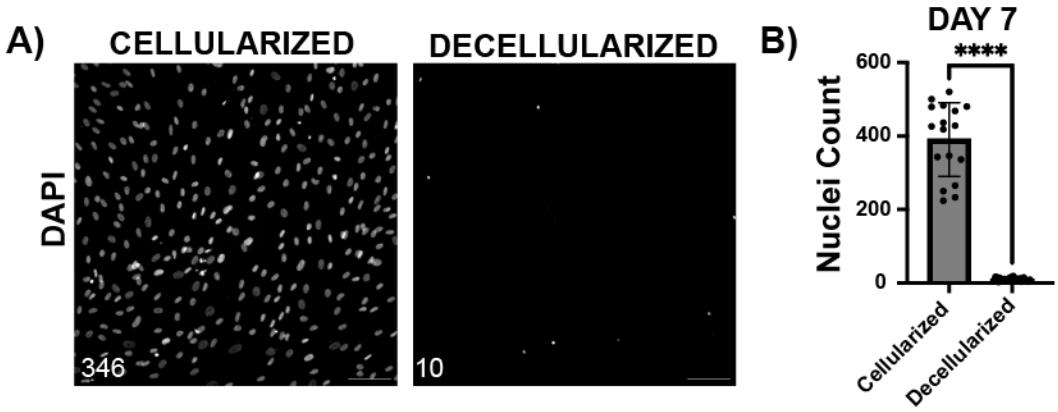

436
437 **Figure S1: Ammonium hydroxide decellularization efficiently clears nuclear material**.
438 Adherent 3D UC MSC cultures were decellularized using an ammonium hydroxide protocol. A)
439 Nuclei were labeled using DAPI and quantified (number in the bottom left of the image). B) The
440 number of nuclei was significantly reduced by 95.8% after decellularization.
441 Representative data from n=3 independent experiments. Scale bar = 100µm..

442 **References**

443 Aisenbrey, E. A., & Murphy, W. L. (2020). Synthetic alternatives to Matrigel. *Nature Reviews.*
444 *Materials*, *5*(7), 539–551. https://doi.org/10.1038/s41578-020-0199-8

445 Assunção, M., Wong, C. W., Richardson, J. J., Tsang, R., Beyer, S., Raghunath, M., & Blocki, A.
446 (2020). Macromolecular dextran sulfate facilitates extracellular matrix deposition by
447 electrostatic interaction independent from a macromolecular crowding effect. *Materials*
448 *Science & Engineering. C, Materials for Biological Applications*, *106*, 110280.
449 https://doi.org/10.1016/j.msec.2019.110280

450 Baker, B. M., & Chen, C. S. (2012). Deconstructing the third dimension – how 3D culture
451 microenvironments alter cellular cues. *Journal of Cell Science*, *125*(13), 3015–3024.
452 https://doi.org/10.1242/jcs.079509

453 Baker, M. (2016a). 1,500 scientists lift the lid on reproducibility. *Nature*, *533*(7604), 452–454.
454 https://doi.org/10.1038/533452a

455 Baker, M. (2016b). Reproducibility: Respect your cells! *Nature*, *537*(7620), 433–435.
456 https://doi.org/10.1038/537433a

457 Bartosh, T. J., Ylöstalo, J. H., Mohammadipoor, A., Bazhanov, N., Coble, K., Claypool, K., Lee, R.
458 H., Choi, H., & Prockop, D. J. (2010). Aggregation of human mesenchymal stromal cells
459 (MSCs) into 3D spheroids enhances their antiinflammatory properties. *Proceedings of the*
460 *National Academy of Sciences*, *107*(31), 13724–13729.
461 https://doi.org/10.1073/pnas.1008117107

462 Black, L. D., Allen, P. G., Morris, S. M., Stone, P. J., & Suki, B. (2008). Mechanical and Failure
463 Properties of Extracellular Matrix Sheets as a Function of Structural Protein Composition.
464 *Biophysical Journal*, *94*(5), 1916–1929. https://doi.org/10.1529/biophysj.107.107144

465 Caplan, A. I. (2017). New MSC: MSCs as pericytes are Sentinels and gatekeepers. *Journal of*
466 *Orthopaedic Research: Official Publication of the Orthopaedic Research Society*, *35*(6),
467 1151–1159. https://doi.org/10.1002/jor.23560
468 Catarino, C. M., Kaiser, K., Baltazar, T., Catarino, L. M., Brewer, J. R., & Karande, P. (2022).
469 Evaluation of native and non-native biomaterials for engineering human skin tissue.
470 *Bioengineering & Translational Medicine*, *7*(3), e10297. https://doi.org/10.1002/btm2.10297
471 Cesarz, Z., & Tamama, K. (2016). Spheroid Culture of Mesenchymal Stem Cells. *Stem Cells*
472 *International*, *2016*, 9176357. https://doi.org/10.1155/2016/9176357
473 Chan, E. C., Kuo, S.-M., Kong, A. M., Morrison, W. A., Dusting, G. J., Mitchell, G. M., Lim, S. Y.,
474 & Liu, G.-S. (2016). Three Dimensional Collagen Scaffold Promotes Intrinsic Vascularisation
475 for Tissue Engineering Applications. *PLOS ONE*, *11*(2), e0149799.
476 https://doi.org/10.1371/journal.pone.0149799
477 Chen, G. H., Sia, K.-C., Liu, S.-W., Kao, Y.-C., Yang, P.-C., Ho, C.-H., Huang, S.-C., Lee, P.-Y.,
478 Liang, M.-Z., Chen, L., & Huang, C.-C. (2025). Implantation of MSC spheroid-derived 3D
479 decellularized ECM enriched with the MSC secretome ameliorates traumatic brain injury and
480 promotes brain repair. *Biomaterials*, *315*, 122941.
481 https://doi.org/10.1016/j.biomaterials.2024.122941
482 Chiang, C.-E., Fang, Y.-Q., Ho, C.-T., Assunção, M., Lin, S.-J., Wang, Y.-C., Blocki, A., & Huang,
483 C.-C. (2021). Bioactive Decellularized Extracellular Matrix Derived from 3D Stem Cell
484 Spheroids under Macromolecular Crowding Serves as a Scaffold for Tissue Engineering.
485 *Advanced Healthcare Materials*, *10*(11), e2100024. https://doi.org/10.1002/adhm.202100024
486 Choi, J., Choi, W., Joo, Y., Chung, H., Kim, D., Oh, S. J., & Kim, S.-H. (2021). FGF2-primed 3D
487 spheroids producing IL-8 promote therapeutic angiogenesis in murine hindlimb ischemia.
488 *NPJ Regenerative Medicine*, *6*, 48. https://doi.org/10.1038/s41536-021-00159-7

489 Corselli, M., Crisan, M., Murray, I. R., West, C. C., Scholes, J., Codrea, F., Khan, N., & Péault, B.
490 (2013). Identification of perivascular mesenchymal stromal/stem cells by flow cytometry.
491 *Cytometry. Part A: The Journal of the International Society for Analytical Cytology*, *83*(8),
492 714–720. https://doi.org/10.1002/cyto.a.22313
493 Crapo, P. M., Gilbert, T. W., & Badylak, S. F. (2011). An overview of tissue and whole organ
494 decellularization processes. *Biomaterials*, *32*(12), 3233–3243.
495 https://doi.org/10.1016/j.biomaterials.2011.01.057
496 de la Vega, L., Lee, C., Sharma, R., Amereh, M., & Willerth, S. M. (2019). 3D bioprinting models of
497 neural tissues: The current state of the field and future directions. *Brain Research Bulletin*,
498 *150*, 240–249. https://doi.org/10.1016/j.brainresbull.2019.06.007
499 Dennis, J. E., Whitney, G. A., Rai, J., Fernandes, R. J., & Kean, T. J. (2020). Physioxia Stimulates
500 Extracellular Matrix Deposition and Increases Mechanical Properties of Human Chondrocyte-
501 Derived Tissue-Engineered Cartilage. *Frontiers in Bioengineering and Biotechnology*, *8*.
502 https://doi.org/10.3389/fbioe.2020.590743
503 Domnina, A., Ivanova, J., Alekseenko, L., Kozhukharova, I., Borodkina, A., Pugovkina, N.,
504 Smirnova, I., Lyublinskaya, O., Fridlyanskaya, I., & Nikolsky, N. (2020). Three-Dimensional
505 Compaction Switches Stress Response Programs and Enhances Therapeutic Efficacy of
506 Endometrial Mesenchymal Stem/Stromal Cells. *Frontiers in Cell and Developmental*
507 *Biology*, *8*, 473. https://doi.org/10.3389/fcell.2020.00473
508 Duisit, J., Amiel, H., Wüthrich, T., Taddeo, A., Dedriche, A., Destoop, V., Pardoen, T., Bouzin, C.,
509 Joris, V., Magee, D., Vögelin, E., Harriman, D., Dessy, C., Orlando, G., Behets, C., Rieben,
510 R., Gianello, P., & Lengelé, B. (2018). Perfusion-decellularization of human ear grafts
511 enables ECM-based scaffolds for auricular vascularized composite tissue engineering. *Acta*
512 *Biomaterialia*, *73*, 339–354. https://doi.org/10.1016/j.actbio.2018.04.009

513 Efremov, Y. M., Zurina, I. M., Presniakova, V. S., Kosheleva, N. V., Butnaru, D. V., Svistunov, A.
514 A., Rochev, Y. A., & Timashev, P. S. (2021). Mechanical properties of cell sheets and
515 spheroids: The link between single cells and complex tissues. *Biophysical Reviews*, *13*(4),
516 541–561. https://doi.org/10.1007/s12551-021-00821-w
517 Fonseca, V. C., Van, V., & Ip, B. C. (2023). *Primary Human Cell-Derived Extracellular Matrix from*
518 *Decellularized Fibroblast Microtissues with Tissue-Dependent Composition and*
519 *Microstructure* (p. 2023.08.15.553420). bioRxiv. https://doi.org/10.1101/2023.08.15.553420
520 Franco-Barraza, J., Beacham, D. A., Amatangelo, M. D., & Cukierman, E. (2016). Preparation of
521 Extracellular Matrices Produced by Cultured and Primary Fibroblasts. *Current Protocols in*
522 *Cell Biology*, *71*, 10.9.1-10.9.34. https://doi.org/10.1002/cpcb.2
523 Fuentes, P., Torres, M. J., Arancibia, R., Aulestia, F., Vergara, M., Carrión, F., Osses, N., &
524 Altamirano, C. (2022). Dynamic Culture of Mesenchymal Stromal/Stem Cell Spheroids and
525 Secretion of Paracrine Factors. *Frontiers in Bioengineering and Biotechnology*, *10*, 916229.
526 https://doi.org/10.3389/fbioe.2022.916229
527 Gilpin, A., & Yang, Y. (2017). Decellularization Strategies for Regenerative Medicine: From
528 Processing Techniques to Applications. *BioMed Research International*, *2017*, 9831534.
529 https://doi.org/10.1155/2017/9831534
530 Gonzalez-Fernandez, T., Tenorio, A. J., Saiz, A. M., & Leach, J. K. (2022). Engineered Cell-Secreted
531 Extracellular Matrix Modulates Cell Spheroid Mechanosensing and Amplifies Their
532 Response to Inductive Cues for the Formation of Mineralized Tissues. *Advanced Healthcare*
533 *Materials*, *11*(10), e2102337. https://doi.org/10.1002/adhm.202102337
534 Gonzalez-Fernandez, T., Tierney, E. G., Cunniffe, G. M., O'Brien, F. J., & Kelly, D. J. (2016). Gene
535 Delivery of TGF-β3 and BMP2 in an MSC-Laden Alginate Hydrogel for Articular Cartilage

536 and Endochondral Bone Tissue Engineering. *Tissue Engineering. Part A*, *22*(9–10), 776–787.
537 https://doi.org/10.1089/ten.TEA.2015.0576
538 Griffith, B. P., Goerlich, C. E., Singh, A. K., Rothblatt, M., Lau, C. L., Shah, A., Lorber, M.,
539 Grazioli, A., Saharia, K. K., Hong, S. N., Joseph, S. M., Ayares, D., & Mohiuddin, M. M.
540 (2022). Genetically Modified Porcine-to-Human Cardiac Xenotransplantation. *New England*
541 *Journal of Medicine*, *387*(1), 35–44. https://doi.org/10.1056/NEJMoa2201422
542 Hemeda, H., Giebel, B., & Wagner, W. (2014). Evaluation of human platelet lysate versus fetal
543 bovine serum for culture of mesenchymal stromal cells. *Cytotherapy*, *16*(2), 170–180.
544 https://doi.org/10.1016/j.jcyt.2013.11.004
545 Huang, J., Zhang, L., Wan, D., Zhou, L., Zheng, S., Lin, S., & Qiao, Y. (2021). Extracellular matrix
546 and its therapeutic potential for cancer treatment. *Signal Transduction and Targeted Therapy*,
547 *6*, 153. https://doi.org/10.1038/s41392-021-00544-0
548 Hughes, C. S., Postovit, L. M., & Lajoie, G. A. (2010). Matrigel: A complex protein mixture required
549 for optimal growth of cell culture. *Proteomics*, *10*(9), 1886–1890.
550 https://doi.org/10.1002/pmic.200900758
551 Jahin, I., Phillips, T., Marcotti, S., Gorey, M.-A., Cox, S., & Parsons, M. (2023). Extracellular matrix
552 stiffness activates mechanosensitive signals but limits breast cancer cell spheroid proliferation
553 and invasion. *Frontiers in Cell and Developmental Biology*, *11*.
554 https://doi.org/10.3389/fcell.2023.1292775
555 Jain, P., Rauer, S. B., Möller, M., & Singh, S. (2022). Mimicking the Natural Basement Membrane
556 for Advanced Tissue Engineering. *Biomacromolecules*, *23*(8), 3081–3103.
557 https://doi.org/10.1021/acs.biomac.2c00402
558 Jin, Y., Kim, H., Min, S., Choi, Y. S., Seo, S. J., Jeong, E., Kim, S. K., Lee, H.-A., Jo, S.-H., Park, J.-
559 H., Park, B.-W., Sim, W.-S., Kim, J.-J., Ban, K., Kim, Y.-G., Park, H.-J., & Cho, S.-W.

560 (2022). Three-dimensional heart extracellular matrix enhances chemically induced direct
561 cardiac reprogramming. *Science Advances*, *8*(50), eabn5768.
562 https://doi.org/10.1126/sciadv.abn5768
563 Johnson, T. D., Hill, R. C., Dzieciatkowska, M., Nigam, V., Behfar, A., Christman, K. L., & Hansen,
564 K. C. (2016). Quantification of Decellularized Human Myocardial Matrix: A Comparison of
565 Six Patients. *Proteomics. Clinical Applications*, *10*(1), 75–83.
566 https://doi.org/10.1002/prca.201500048
567 Jung, S., Sen, A., Rosenberg, L., & Behie, L. A. (2010). Identification of growth and attachment
568 factors for the serum-free isolation and expansion of human mesenchymal stromal cells.
569 *Cytotherapy*, *12*(5), 637–657. https://doi.org/10.3109/14653249.2010.495113
570 Kane, K. I. W., Lucumi Moreno, E., Lehr, C. M., Hachi, S., Dannert, R., Sanctuary, R., Wagner, C.,
571 Fleming, R. M. T., & Baller, J. (2018). Determination of the rheological properties of
572 Matrigel for optimum seeding conditions in microfluidic cell cultures. *AIP Advances*, *8*(12),
573 125332. https://doi.org/10.1063/1.5067382
574 Kang, S.-G., Shinojima, N., Hossain, A., Gumin, J., Yong, R. L., Colman, H., Marini, F., Andreeff,
575 M., & Lang, F. F. (2010). Isolation and Perivascular Localization of Mesenchymal Stem Cells
576 From Mouse Brain. *Neurosurgery*, *67*(3), 711–720.
577 https://doi.org/10.1227/01.NEU.0000377859.06219.78
578 Keppie, S. J., Mansfield, J. C., Tang, X., Philp, C. J., Graham, H. K., Önnerfjord, P., Wall, A.,
579 McLean, C., Winlove, C. P., Sherratt, M. J., Pavlovskaya, G. E., & Vincent, T. L. (2021).
580 Matrix-Bound Growth Factors are Released upon Cartilage Compression by an Aggrecan-
581 Dependent Sodium Flux that is Lost in Osteoarthritis. *Function*, *2*(5), zqab037.
582 https://doi.org/10.1093/function/zqab037

583 Khalilgharibi, N., & Mao, Y. (2021). To form and function: On the role of basement membrane
584 mechanics in tissue development, homeostasis and disease. *Open Biology*, *11*(2), 200360.
585 https://doi.org/10.1098/rsob.200360
586 Kim, M.-H., Tan, S. Y., Yamahara, K., & Kino-oka, M. (2023). An *in vitro* culture platform to study
587 the extracellular matrix remodeling potential of human mesenchymal stem cells. *Acta*
588 *Biomaterialia*, *170*, 376–388. https://doi.org/10.1016/j.actbio.2023.08.035
589 Kleinman, H. K., & Martin, G. R. (2005). Matrigel: Basement membrane matrix with biological
590 activity. *Seminars in Cancer Biology*, *15*(5), 378–386.
591 https://doi.org/10.1016/j.semcancer.2005.05.004
592 Kosheleva, N. V., Efremov, Y. M., Koteneva, P. I., Ilina, I. V., Zurina, I. M., Bikmulina, P. Y.,
593 Shpichka, A. I., & Timashev, P. S. (2023). Building a tissue: Mesenchymal and epithelial cell
594 spheroids mechanical properties at micro- and nanoscale. *Acta Biomaterialia*, *165*, 140–152.
595 https://doi.org/10.1016/j.actbio.2022.09.051
596 Kozlowski, M. T., Crook, C. J., & Ku, H. T. (2021). Towards organoid culture without Matrigel.
597 *Communications Biology*, *4*(1), 1387. https://doi.org/10.1038/s42003-021-02910-8
598 Kumada, Y., & Zhang, S. (2010). Significant Type I and Type III Collagen Production from Human
599 Periodontal Ligament Fibroblasts in 3D Peptide Scaffolds without Extra Growth Factors.
600 *PLOS ONE*, *5*(4), e10305. https://doi.org/10.1371/journal.pone.0010305
601 Kumar, P., Satyam, A., Cigognini, D., Pandit, A., & Zeugolis, D. I. (2018). Low oxygen tension and
602 macromolecular crowding accelerate extracellular matrix deposition in human corneal
603 fibroblast culture. *Journal of Tissue Engineering and Regenerative Medicine*, *12*(1), 6–18.
604 https://doi.org/10.1002/term.2283

605 Lee, J. H., Han, Y.-S., & Lee, S. H. (2016). Long-Duration Three-Dimensional Spheroid Culture
606 Promotes Angiogenic Activities of Adipose-Derived Mesenchymal Stem Cells. *Biomolecules*
607 *& Therapeutics*, *24*(3), 260. https://doi.org/10.4062/biomolther.2015.146
608 Li, M., Fu, T., Yang, S., Pan, L., Tang, J., Chen, M., Liang, P., Gao, Z., & Guo, L. (2021). Agarose-
609 based spheroid culture enhanced stemness and promoted odontogenic differentiation potential
610 of human dental follicle cells in vitro. *In Vitro Cellular & Developmental Biology. Animal*,
611 *57*(6), 620–630. https://doi.org/10.1007/s11626-021-00591-5
612 Liu, S., Yang, W., Li, Y., & Sun, C. (2023). Fetal bovine serum, an important factor affecting the
613 reproducibility of cell experiments. *Scientific Reports*, *13*, 1942.
614 https://doi.org/10.1038/s41598-023-29060-7
615 Maia, F. R., Fonseca, K. B., Rodrigues, G., Granja, P. L., & Barrias, C. C. (2014). Matrix-driven
616 formation of mesenchymal stem cell–extracellular matrix microtissues on soft alginate
617 hydrogels. *Acta Biomaterialia*, *10*(7), 3197–3208.
618 https://doi.org/10.1016/j.actbio.2014.02.049
619 Malakpour-Permlid, A., Buzzi, I., Hegardt, C., Johansson, F., & Oredsson, S. (2021). Identification
620 of extracellular matrix proteins secreted by human dermal fibroblasts cultured in 3D
621 electrospun scaffolds. *Scientific Reports*, *11*(1), 6655. https://doi.org/10.1038/s41598-021-
622 85742-0
623 Marinkovic, M., Block, T. J., Rakian, R., Li, Q., Wang, E., Reilly, M. A., Dean, D. D., & Chen, X.-
624 D. (2016). One size does not fit all: Developing a cell-specific niche for in vitro study of cell
625 behavior. *Matrix Biology : Journal of the International Society for Matrix Biology*, *52–54*,
626 426–441. https://doi.org/10.1016/j.matbio.2016.01.004
627 Marinkovic, M., Tran, O. N., Block, T. J., Rakian, R., Gonzalez, A. O., Dean, D. D., Yeh, C.-K., &
628 Chen, X.-D. (2020). Native extracellular matrix, synthesized ex vivo by bone marrow or

629 adipose stromal cells, faithfully directs mesenchymal stem cell differentiation. *Matrix Biology*
630 *Plus*, *8*, 100044. https://doi.org/10.1016/j.mbplus.2020.100044
631 Marrella, A., Lee, T. Y., Lee, D. H., Karuthedom, S., Syla, D., Chawla, A., Khademhosseini, A., &
632 Jang, H. L. (2018). Engineering vascularized and innervated bone biomaterials for improved
633 skeletal tissue regeneration. *Materials Today*, *21*(4), 362–376.
634 https://doi.org/10.1016/j.mattod.2017.10.005
635 Minor, A. J., & Coulombe, K. L. K. (2020). Engineering a collagen matrix for cell-instructive
636 regenerative angiogenesis. *Journal of Biomedical Materials Research Part B: Applied*
637 *Biomaterials*, *108*(6), 2407–2416. https://doi.org/10.1002/jbm.b.34573
638 Motta, L. C. B., Pereira, V. M., Pinto, P. A. F., Mançanares, C. A. F., Pieri, N. C. G., de Olveira, V.
639 C., Fantinato-Neto, P., & Ambrósio, C. E. (2023). 3D culture of mesenchymal stem cells
640 from the yolk sac to generate intestinal organoid. *Theriogenology*, *209*.
641 https://doi.org/10.1016/j.theriogenology.2023.06.003
642 Murphy, K. C., Hung, B. P., Browne-Bourne, S., Zhou, D., Yeung, J., Genetos, D. C., & Leach, J. K.
643 (2017). Measurement of oxygen tension within mesenchymal stem cell spheroids. *Journal of*
644 *The Royal Society Interface*, *14*(127), 20160851. https://doi.org/10.1098/rsif.2016.0851
645 Naderi-Meshkin, H., Cornelius, V. A., Eleftheriadou, M., Potel, K. N., Setyaningsih, W. A. W., &
646 Margariti, A. (2023). Vascular organoids: Unveiling advantages, applications, challenges, and
647 disease modelling strategies. *Stem Cell Research & Therapy*, *14*(1), 292.
648 https://doi.org/10.1186/s13287-023-03521-2
649 Novoseletskaya, E., Grigorieva, O., Nimiritsky, P., Basalova, N., Eremichev, R., Milovskaya, I.,
650 Kulebyakin, K., Kulebyakina, M., Rodionov, S., Omelyanenko, N., & Efimenko, A. (2020).
651 Mesenchymal Stromal Cell-Produced Components of Extracellular Matrix Potentiate

652 Multipotent Stem Cell Response to Differentiation Stimuli. *Frontiers in Cell and*
653 *Developmental Biology*, *8*, 555378. https://doi.org/10.3389/fcell.2020.555378
654 Olesen, K., Rodin, S., Mak, W. C., Felldin, U., Österholm, C., Tilevik, A., & Grinnemo, K.-H.
655 (2021). Spatiotemporal Extracellular Matrix Modeling for in Situ Cell Niche Studies. *Stem*
656 *Cells*, *39*(12), 1751–1765. https://doi.org/10.1002/stem.3448
657 Park, J., Kim, J., Sullivan, K. M., Baik, S., Ko, E., Kim, M.-J., Kim, Y. J., & Kong, H. (2018).
658 Decellularized Matrix Produced by Mesenchymal Stem Cells Modulates Growth and
659 Metabolic Activity of Hepatic Cell Cluster. *ACS Biomaterials Science & Engineering*, *4*(2),
660 456–462. https://doi.org/10.1021/acsbiomaterials.7b00494
661 Perugini, V., & Santin, M. (2021). A Substrate-Mimicking Basement Membrane Drives the
662 Organization of Human Mesenchymal Stromal Cells and Endothelial Cells Into Perivascular
663 Niche-Like Structures. *Frontiers in Cell and Developmental Biology*, *9*, 701842.
664 https://doi.org/10.3389/fcell.2021.701842
665 Pompili, S., Latella, G., Gaudio, E., Sferra, R., & Vetuschi, A. (2021). The Charming World of the
666 Extracellular Matrix: A Dynamic and Protective Network of the Intestinal Wall. *Frontiers in*
667 *Medicine*, *8*. https://doi.org/10.3389/fmed.2021.610189
668 Prewitz, M. C., Seib, F. P., von Bonin, M., Friedrichs, J., Stißel, A., Niehage, C., Müller, K.,
669 Anastassiadis, K., Waskow, C., Hoflack, B., Bornhäuser, M., & Werner, C. (2013). Tightly
670 anchored tissue-mimetic matrices as instructive stem cell microenvironments. *Nature*
671 *Methods*, *10*(8), 788–794. https://doi.org/10.1038/nmeth.2523
672 Rakian, R., Block, T. J., Johnson, S. M., Marinkovic, M., Wu, J., Dai, Q., Dean, D. D., & Chen, X.-
673 D. (2015). Native extracellular matrix preserves mesenchymal stem cell "stemness" and
674 differentiation potential under serum-free culture conditions. *Stem Cell Research & Therapy*,
675 *6*, 235. https://doi.org/10.1186/s13287-015-0235-6

676 Sagaradze, G. D., Basalova, N. A., Efimenko, A. Y., & Tkachuk, V. A. (2020). Mesenchymal
677 Stromal Cells as Critical Contributors to Tissue Regeneration. *Frontiers in Cell and*
678 *Developmental Biology*, *8*. https://doi.org/10.3389/fcell.2020.576176
679 Saraswathibhatla, A., Indana, D., & Chaudhuri, O. (2023). Cell–extracellular matrix
680 mechanotransduction in 3D. *Nature Reviews. Molecular Cell Biology*, *24*(7), 495–516.
681 https://doi.org/10.1038/s41580-023-00583-1
682 Satyam, A., Kumar, P., Cigognini, D., Pandit, A., & Zeugolis, D. I. (2016). Low, but not too low,
683 oxygen tension and macromolecular crowding accelerate extracellular matrix deposition in
684 human dermal fibroblast culture. *Acta Biomaterialia*, *44*, 221–231.
685 https://doi.org/10.1016/j.actbio.2016.08.008
686 Schindelin, J., Arganda-Carreras, I., Frise, E., Kaynig, V., Longair, M., Pietzsch, T., Preibisch, S.,
687 Rueden, C., Saalfeld, S., Schmid, B., Tinevez, J.-Y., White, D. J., Hartenstein, V., Eliceiri,
688 K., Tomancak, P., & Cardona, A. (2012). Fiji: An open-source platform for biological-image
689 analysis. *Nature Methods*, *9*(7), 676–682. https://doi.org/10.1038/nmeth.2019
690 Schneider, K. H., Goldberg, B. J., Hasturk, O., Mu, X., Dötzlhofer, M., Eder, G., Theodossiou, S.,
691 Pichelkastner, L., Riess, P., Rohringer, S., Kiss, H., Teuschl-Woller, A. H., Fitzpatrick, V.,
692 Enayati, M., Podesser, B. K., Bergmeister, H., & Kaplan, D. L. (2023). Silk fibroin, gelatin,
693 and human placenta extracellular matrix-based composite hydrogels for 3D bioprinting and
694 soft tissue engineering. *Biomaterials Research*, *27*(1), 117. https://doi.org/10.1186/s40824-
695 023-00431-5
696 Seif-Naraghi, S. B., Horn, D., Schup-Magoffin, P. A., & Christman, K. L. (2012). Injectable
697 extracellular matrix derived hydrogel provides a platform for enhanced retention and delivery
698 of a heparin-binding growth factor. *Acta Biomaterialia*, *8*(10), 3695–3703.
699 https://doi.org/10.1016/j.actbio.2012.06.030

700 Shaheen, M. F., Joo, D., Ross, J. J., Anderson, B. D., Chen, H. S., Huebert, R. C., Li, Y., Amiot, B.,
701 Young, A., Zlochiver, V., Nelson, E., Mounajjed, T., Dietz, A. B., Michalak, G., Steiner, B.
702 G., Davidow, D. S., Paradise, C. R., van Wijnen, A. J., Shah, V. H., … Nyberg, S. L. (2020).
703 Sustained perfusion of revascularized bioengineered livers heterotopically transplanted into
704 immunosuppressed pigs. *Nature Biomedical Engineering*, *4*(4), 437–445.
705 https://doi.org/10.1038/s41551-019-0460-x
706 Shearier, E., Xing, Q., Qian, Z., & Zhao, F. (2016). Physiologically Low Oxygen Enhances
707 Biomolecule Production and Stemness of Mesenchymal Stem Cell Spheroids. *Tissue*
708 *Engineering. Part C, Methods*, *22*(4), 360. https://doi.org/10.1089/ten.tec.2015.0465
709 Smith, A., Huang, M., Watkins, T., Burguin, F., Baskin, J., & Garlick, J. A. (2020). De novo
710 production of human extracellular matrix supports increased throughput and cellular
711 complexity in 3D skin equivalent model. *Journal of Tissue Engineering and Regenerative*
712 *Medicine*, *14*(8), 1019–1027. https://doi.org/10.1002/term.3071
713 Tao, F., Sayo, K., Sugimoto, K., Aoki, S., & Kojima, N. (2020). Development of a tunable method to
714 generate various three-dimensional microstructures by replenishing macromolecules such as
715 extracellular matrix components and polysaccharides. *Scientific Reports*, *10*, 6567.
716 https://doi.org/10.1038/s41598-020-63621-4
717 Thai, V. L., Mierswa, S., Griffin, K. H., Boerckel, J. D., & Leach, J. K. (2024). Mechanoregulation
718 of MSC spheroid immunomodulation. *APL Bioengineering*, *8*(1), 016116.
719 https://doi.org/10.1063/5.0184431
720 Tong, Z., Martyn, K., Yang, A., Yin, X., Mead, B. E., Joshi, N., Sherman, N. E., Langer, R. S., &
721 Karp, J. M. (2018). Towards a defined ECM and small molecule based monolayer culture
722 system for the expansion of mouse and human intestinal stem cells. *Biomaterials*, *154*, 60–73.
723 https://doi.org/10.1016/j.biomaterials.2017.10.038

724 Tuftee, C., Alsberg, E., Ozbolat, I. T., & Rizwan, M. (2024). Emerging granular hydrogel bioinks to
725 improve biological function in bioprinted constructs. *Trends in Biotechnology*, *42*(3), 339–
726 352. https://doi.org/10.1016/j.tibtech.2023.09.007
727 Ushakov, R., Ratushnyy, A., Buravkova, L., Tolkunova, E., & Burova, E. (2024). The Decellularized
728 Cell-Derived Extracellular Matrix Enhances the Paracrine Function of Human Mesenchymal
729 Stromal/Stem Cells. *International Journal of Molecular Sciences*, *25*(4), Article 4.
730 https://doi.org/10.3390/ijms25042419
731 Wiese, D. M., & Braid, L. R. (2020). Transcriptome profiles acquired during cell expansion and
732 licensing validate mesenchymal stromal cell lineage genes. *Stem Cell Research and Therapy*,
733 *11*(1), 1–7. https://doi.org/10.1186/S13287-020-01873-7/FIGURES/3
734 Wiese, D. M., Wood, C. A., Ford, B. N., & Braid, L. R. (2022). Cytokine Activation Reveals Tissue-
735 Imprinted Gene Profiles of Mesenchymal Stromal Cells. *Frontiers in Immunology*, *13*.
736 https://www.frontiersin.org/articles/10.3389/fimmu.2022.917790
737 Wilks, B. T., Evans, E. B., Nakhla, M. N., & Morgan, J. R. (2018). Directing fibroblast self-assembly
738 to fabricate highly-aligned, collagen-rich matrices. *Acta Biomaterialia*, *81*, 70–79.
739 https://doi.org/10.1016/j.actbio.2018.09.030
740 Yang, M. C., Chin, I. L., Fang, H., Drack, A., Nour, S., Choi, Y. S., O'Connor, A. J., Greening, D.
741 W., Kalionis, B., & Heath, D. E. (2024). Tailored environments for directed mesenchymal
742 stromal cell proliferation and differentiation using decellularized extracellular matrices in
743 conjunction with substrate modulus. *Acta Biomaterialia*, *187*, 110–122.
744 https://doi.org/10.1016/j.actbio.2024.08.022
745 Yin, S., Wu, H., Huang, Y., Lu, C., Cui, J., Li, Y., Xue, B., Wu, J., Jiang, C., Gu, X., Wang, W., &
746 Cao, Y. (2024). Structurally and mechanically tuned macroporous hydrogels for scalable

747 mesenchymal stem cell–extracellular matrix spheroid production. *Proceedings of the National*
748 *Academy of Sciences*, *121*(28), e2404210121. https://doi.org/10.1073/pnas.2404210121
749 Zhang, X., Battiston, K. G., Labow, R. S., Simmons, C. A., & Santerre, J. P. (2017). Generating
750 favorable growth factor and protease release profiles to enable extracellular matrix
751 accumulation within an *in vitro* tissue engineering environment. *Acta Biomaterialia*, *54*, 81–
752 94. https://doi.org/10.1016/j.actbio.2017.02.041
753 Zhang, Y., Feng, Y., Shao, Q., Jiang, Z., & Yang, G. (2023). Rapid formation of 3D: Decellularized
754 extracellular matrix spheroids for enhancing bone formation. *Journal of Biomedical Materials*
755 *Research. Part A*, *111*(3), 378–388. https://doi.org/10.1002/jbm.a.37471
756 Zhao, W., Zhu, J., Hang, J., & Zeng, W. (2022). Biomaterials to promote vascularization in tissue
757 engineering organs and ischemic fibrotic diseases. *MedComm – Biomaterials and*
758 *Applications*, *1*(1), e16. https://doi.org/10.1002/mba2.16
759
760
761
762
763
764
765
766
767
768
769
770
771

772